Non-isothermal decomposition kinetics, thermal behavior and computational detonation properties on 4-amino-1,2,4-triazol-5-one (ATO)

ARTICLE *in* JOURNAL OF ANALYTICAL AND APPLIED PYROLYSIS · NOVEMBER 2008

Impact Factor: 3.56 · DOI: 10.1016/j.jaap.2008.07.007

5 AUTHORS, INCLUDING:

Hai-Xia Ma
Northwest University
125 PUBLICATIONS **661** CITATIONS

SEE PROFILE

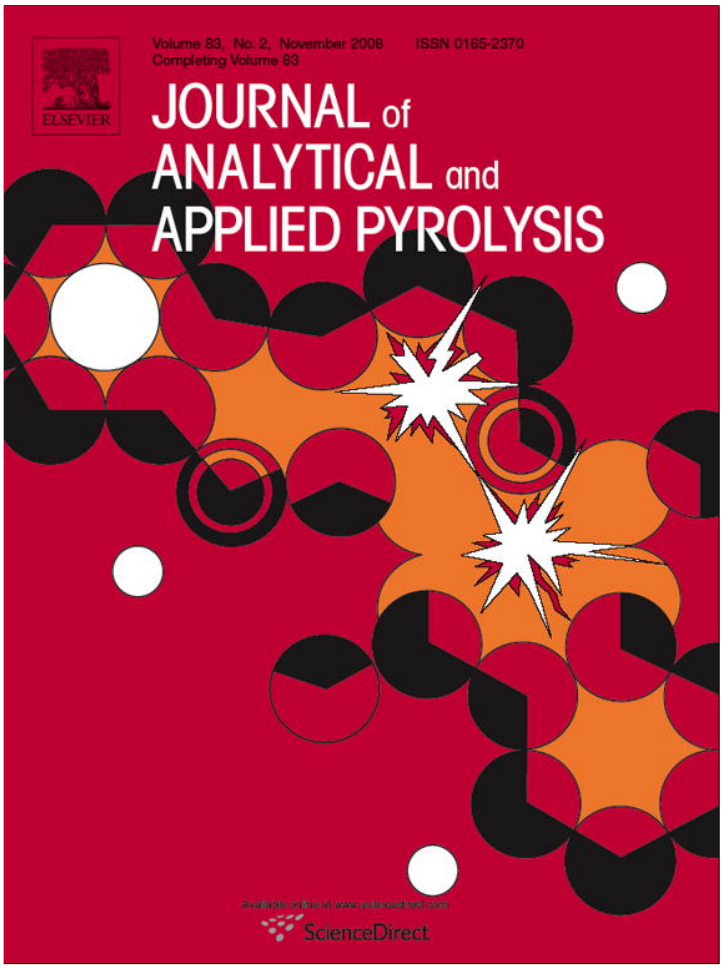

J. Anal. Appl. Pyrolysis 83 (2008) 145–150

Contents lists available at ScienceDirect

Journal of Analytical and Applied Pyrolysis

journal homepage: www.elsevier.com/locate/jaap

Non-isothermal decomposition kinetics, thermal behavior and computational detonation properties on 4-amino-1,2,4-triazol-5-one (ATO)

Hai-Xia Ma [a,*], Ji-Rong Song [a,b,**], Rong-Zu Hu [c], Qing Pan [c], Yuan Wang [c]

[a] College of Chemical Engineering/Shaanxi Key Laboratory of Physico-Inorganic Chemistry, Northwest University, Xi'an, Shaanxi 710069, PR China
[b] Conservation Technology Department, The Palace Museum, 4 Jingshan Qianjie, Beijing 100009, PR China
[c] Xi'an Modern Chemistry Research Institute, Xi'an 710065, PR China

ARTICLE INFO

Article history:
Received 21 February 2008
Accepted 18 July 2008
Available online 3 August 2008

Keywords:
4-Amino-1,2,4-triazol-5-one (ATO)
Decomposition kinetics
Thermal behavior
Detonation properties

ABSTRACT

The thermal behavior of 4-amino-1,2,4-triazol-5-one (ATO) was studied under non-isothermal condition by DSC method in a sealed cell of stainless steel. The melting enthalpy and melting entropy of ATO are 21.34 ± 0.49 kJ mol^{-1} and 46.54 ± 0.30 J mol^{-1} K^{-1}, respectively. The kinetic parameters were obtained from the analysis of DSC curves by Kissinger method, Ozawa method, the differential method and the integral method. The main exothermic decomposition reaction mechanism of ATO is classified as nucleation and growth, and the kinetic parameters of the reaction are $E_a = 119.50$ kJ mol^{-1} and $A = 10^{9.03}$ s^{-1}. The gas products and condensed phase products of the thermal decomposition of ATO were studied on two simultaneous devices of the fast thermolysis reaction cell (gas reaction cell) *in situ* in conjunction with rapid scan transform infrared spectroscopy (RSFT-IR) and the solid reaction cell *in situ*. The heat of formation (HOF) for ATO was evaluated by G3 theory. The detonation velocity (D) and detonation pressure (P) were estimated by using the well-known Kamlet–Jacobs equation, based on the theoretical HOF and the determined crystal density.

1. Introduction

Some of the nitrogen heterocyclic ring compounds have been utilized in energetic roles due to higher heats of formation (HOF), density and oxygen balance than those of their carboxylic analogues such as 4-amino-1,2,4-triazol-5-one (ATO). In 1964, Kroeger et al. [1] first prepared ATO using carbohydrazide. Odenthal and co-workers [2–4] synthesized a series of ATO derivatives. The molecular fragments of 25 kinds of ATO and its derivatives were analyzed by Bernardini and Vialleofont [5] using mass spectrometry.

This triazolone compound can easily coordinate with metals due to the presence of lone electron pairs on the oxygen atom of the carbonyl group, the nitrogen atom of the amino group and the nitrogen atom of the five-member ring. Therefore, ATO have been used to prepare energetic complexes [6–9] besides its potential usage in energetic explosives as an intermediate [9].

Zhang and Zhang [10] described that the thermal decomposition process of ATO was composed of one melting peak (the peak temperature T_p is 180.2 °C) and one endothermic decomposition peak with $T_p = 234.1$ °C by performing the result on a CDR-1 Instrument at a heating rate of 10.00 °C min^{-1} with α-Al_2O_3 as the reference sample. The flash pyrolysis of ATO was investigated by T-Jump FT-IR spectroscopy and the main gaseous remains were HCHO, NH_3, HCN, H_2O and NO_2. We have synthesized the single crystal of ATO, reported its molecular structure, and made a density-functional theoretical investigation on its dimers and crystal band structure [11]. In this paper, we determined its gas products and condensed phase products under two simultaneous device of the fast thermolysis reaction cell (gas reaction cell) *in situ* in conjunction with rapid scan transform infrared spectroscopy (RSFT-IR) and the solid reaction cell *in situ*. The DSC experimental was also carried out on a CDR-4P Instrument with sealed stainless steel cells and the result was different with that of Zhang and Zhang's, which is described in Section 3.1. The non-isothermal reaction kinetics of the thermal decomposition reaction was also investigated. This is quite useful in the evaluation of its thermal stability under non-isothermal condition and in the analysis of compatibility of energetic materials. The performance of ATO as an energetic material, including heat formation, the detonation velocity and detonation pressure were investigated.

* Corresponding author at: College of Chemical Engineering, Northwest University, Xi'an, Shaanxi 710069, PR China.
** Corresponding author at: Conservation Technology Department, The Palace Museum, 4 Jingshan Qianjie, Beijing 100009, PR China.
E-mail addresses: mahx@nwu.edu.cn (H.-X. Ma), songji@nwu.edu.cn (J.-R. Song).

0165-2370/$ – see front matter © 2008 Elsevier B.V. All rights reserved.
doi:10.1016/j.jaap.2008.07.007

2. Experimental and computational methods

2.1. Sample

ATO used in this work was prepared according to the literature [11]. Anal. Calcd. (%) for $C_2H_4N_4O$: C 24.00, N 55.98, H 4.03; found (%): C 24.30, N 55.36, H 3.94. IR (KBr): $\nu^{s}_{-NH-H} = 3331\,cm^{-1}$, $\nu^{as}_{-NH-H} = 3304\,cm^{-1}$, $\nu^{s}_{N-H} = 3201\,cm^{-1}$, $\delta_{N-H} = 1643\,cm^{-1}$, $\delta_{N-H} = 695\,cm^{-1}$, $\nu^{s}_{=C-H} = 3073\,cm^{-1}$, $\nu^{s}_{C=O} = 1710\,cm^{-1}$, $\nu^{s}_{C=N} = 1571\,cm^{-1}$, $\nu^{S}_{C-N} = 1249\,cm^{-1}$. ^{13}C NMR (400 MHz, D_2O, ppm) δ: 157.862 (C=O), δ: 142.602 (C–H), ^{1}H NMR (400 MHz, D_2O, ppm) δ: 7.868 (CH). Sample was kept in a vacuum desiccator before use.

2.2. Equipments

The elemental analysis was measured on a PE-2400 elemental analytical instrument (PerkinElmer, USA) and IR on a Nicolet 60 SXR FT-IR (Nicolet, USA) spectrometer in the 4000–400 cm^{-1} region using KBr pellets. ^{1}H NMR and ^{13}C NMR spectra were recorded on an INOVA-400 NMR (VARIAN, USA) spectrometer using D_2O as the solvent.

2.3. Thermal decomposition condition

The DSC experiments were carried out on a CDR-4P Instrument (Shanghai Balance Manufacturer, P. R. China) with sealed stainless steel cells at heating rates of 5.85, 12.07, 18.12 and 24.94 °C min^{-1} from ambient temperature to 400 °C in a static atmosphere. The temperature and heat were calibrated using pure indium and tin particles. The DSC curves obtained under the same conditions overlap with each other, indicating that the reproducibility of tests was satisfactory.

Thermolysis/RSFT-IR measurements were conducted using a model NEXUS 870 FT-IR spectrophotometer (Nicolet Instruments Co., USA) and *in situ* thermolysis cell (Xiamen University, China) with the temperature range of 20–375 °C at a heating rate of 10 °C min^{-1} with a KBr pellet sample (about 0.7 mg of ATO and 150 mg of KBr). IR spectra of ATO in the range of 4000–400 cm^{-1} were acquired by a model DTGS detector at a rate of 8.8 files min^{-1} and 16 scans $file^{-1}$ with a resolution of 4 cm^{-1}.

The main gaseous products were determined by the T-Jump/FT-IR, which was used on a Nicolet 60 SXR FT-IR spectrometer equipped with an MCT-A detector at a rate of 5 files s^{-1}, 2 scans $file^{-1}$ with a resolution of 8 cm^{-1}. The detector was heated to 700 °C at a heating rate of 700 °C s^{-1}.

2.4. The method of computing detonation properties

Heat of formation (HOF) of ATO was evaluated by G3 theory, based on the atomization energies being used by Curtiss et al. [12]. All calculations were carried out on an IBM P4 computer with Gaussian-03W [13] program.

The empirical Kamlet–Jacobs equation [14] is widely applied to estimate the values of D and P for the explosives containing C, H, O and N as following:

$$D = 0.7062(NM^{1/2}Q^{1/2})^{1/2}(1 + 1.30\rho) \quad (1)$$

$$P = 7.167 \times 10^{8} NM^{1/2}Q^{1/2}\rho^{2} \quad (2)$$

where each term in Eqs. (1) and (2) is defined as follows: D, detonation velocity (km/s); P, detonation pressure (GPa); N, moles of gases detonation products per gram of explosive; M, average molecular weight of gaseous products; Q, chemical energy of detonation (J g^{-1}); and ρ, density of explosives (g cm^{-3}).

3. Results and discussion

3.1. Thermal behavior of ATO

Typical DSC curve of ATO is shown in Fig. 1. DSC curve of ATO exhibits one endothermic and one exothermic peak. The extrapolated onset temperature (T_e), peak temperature (T_m), melting enthalpy (ΔH_m) and melting entropy (ΔS_m) of the melting process of ATO obtained by six measurements are 185.39 ± 0.42 °C, 188.10 ± 0.47 °C, 21.34 ± 0.49 kJ mol^{-1} and 46.54 ± 0.30 J mol^{-1} K^{-1}, respectively. The exothermic peak temperature is 317.34 °C, which is different from the results of Zhang and Zhang.

3.2. Analysis of kinetic data for the exothermic main decomposition reaction of the compound

In order to obtain the kinetic parameters (the apparent activation energy (E_a) and pre-exponential constant (A)) of the main decomposition reaction for ATO, a multiple heating method (Kissinger method [15] and Ozawa method [16]) was employed. The Kissinger and Ozawa equations are as follows:

$$\frac{d\ln(\beta/T_p^2)}{d(1/T_p)} = -\frac{E_a}{R} \quad (3)$$

$$\log\beta + \frac{0.4567E_a}{RT} = C \quad (4)$$

where T is the absolute temperature, T_P is the peak temperature, R is the gas constant, E_a is the apparent activation energy, β is the linear heating rate and C is a constant.

The integral Eqs. (5)–(8) and differential Eq. (9) are cited to obtain the values of E_a, A and the most probable kinetic model function [$f(\alpha)$] from a single non-isothermal DSC curve [17].

MacCallum–Tanner equation:

$$\log[G(\alpha)] = \log\left(\frac{AE_a}{\beta R}\right) - 0.4828E_a^{0.4357} - \frac{0.449 + 0.217E_a}{0.001}\frac{1}{T} \quad (5)$$

Satava–Sestak equation:

$$\log[G(\alpha)] = \log\left(\frac{AE_a}{\beta R}\right) - 2.315 - 0.4567\frac{E_a}{RT} \quad (6)$$

The general integral equation:

$$\ln\left[\frac{G(\alpha)}{T - T_0}\right] = \ln\left(\frac{A}{\beta}\right) - \frac{E_a}{RT} \quad (7)$$

Agrawal equation:

$$\ln\left[\frac{G(\alpha)}{T^2}\right] = \ln\left\{\left(\frac{AR}{\beta E_a}\right)\left[\frac{1 - 2(RT/E_a)}{1 - 5(RT/E_a)^2}\right]\right\} - \frac{E_a}{RT} \quad (8)$$

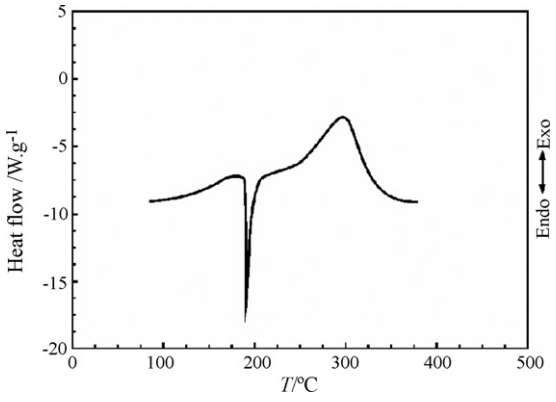

Fig. 1. DSC curve of ATO at a heating rate of 12.07 °C min^{-1} in sealed cells of stainless steel.

Table 1
Base data of ATO determined by DSC curve (β = 12.07 °C min^{-1})

Data point	T (K)	α	dH/dt (mJ s^{-1})	Data point	T (K)	α	dH/dt (mJ s^{-1})
1	532.27	0.0610	1.251	29	560.17	0.4490	3.656
2	534.07	0.0771	1.343	30	561.07	0.4560	3.689
3	535.27	0.0837	1.427	31	561.67	0.4805	3.698
4	536.77	0.1046	1.581	32	562.27	0.4934	3.733
5	538.27	0.1185	1.740	33	562.87	0.5056	3.778
6	539.47	0.1254	1.777	34	563.47	0.5194	3.802
7	540.67	0.1429	1.891	35	563.77	0.5258	3.841
8	541.87	0.1556	1.992	36	564.37	0.5380	3.879
9	543.07	0.1651	2.045	37	564.67	0.5461	3.867
10	544.27	0.1839	2.174	38	564.97	0.5520	3.898
11	545.47	0.1998	2.283	39	566.77	0.5793	3.905
12	546.67	0.2064	2.337	40	567.07	0.5800	3.902
13	547.87	0.2323	2.541	41	567.67	0.6131	3.955
14	548.77	0.2462	2.659	42	568.27	0.6245	3.944
15	549.67	0.2591	2.721	43	568.87	0.6388	3.961
16	550.57	0.2677	2.772	44	569.17	0.6438	3.935
17	551.47	0.2883	2.897	45	570.07	0.6505	3.948
18	552.37	0.3027	2.949	46	570.67	0.6795	3.912
19	553.27	0.3196	3.014	47	570.97	0.6860	3.902
20	553.87	0.3282	3.090	48	571.27	0.6927	3.893
21	554.47	0.3385	3.122	49	571.87	0.7051	3.863
22	555.07	0.3449	3.163	50	572.17	0.7126	3.890
23	556.57	0.3788	3.321	51	572.77	0.7262	3.857
24	557.47	0.3944	3.433	52	573.07	0.7326	3.806
25	558.07	0.4060	3.506	53	573.67	0.7454	3.775
26	558.67	0.4192	3.556	54	574.27	0.7524	3.759
27	558.97	0.4240	3.570	55	576.37	0.7836	3.607
28	559.27	0.4301	3.597	56	576.67	0.8103	3.468

The initial temperature (T_0) is 236.92 °C, H_0 = 390.72 mJ, the sample mass (m_s) is 0.5200 mg.

Achar–Brindley–Sharp equation:

$$\ln\left[\frac{\mathrm{d}\alpha}{f(\alpha)\,\mathrm{d}T}\right] = \ln\left(\frac{A}{\beta}\right) - \frac{E_a}{RT}\left(\frac{\mathrm{d}\alpha}{\mathrm{d}t} = \beta\frac{\mathrm{d}\alpha}{\mathrm{d}T}\right) \tag{9}$$

where $f(\alpha)$ and $G(\alpha)$ are the differential model function and the integral model function, respectively, dα/dt is the rate of conversion, dα/dT = (1/$H_0\beta$)(dH/dt), (dH/dt) the exothermic heat flow at time t, H_0 the total heat effect (corresponding to the global area under the DSC curve), T the temperature (K) at time t, α the conversion degree, R the gas constant.

Forty-one types of kinetic model functions (Appendix A) in Ref. [18] and the original 56 data selected from the DSC curve were tabulated in Table 1 and put into Eqs. (5)–(9) for calculation, respectively. The kinetic parameters and the probable kinetic model function was selected by the logical choice method [17,18] and satisfying the ordinary range of the thermal decomposition kinetic parameters for energetic materials (E_a = 80–250 kJ mol^{-1}, log A = 7–30 s^{-1}) together with their appropriate values of linear correlation coefficient (r), are presented in Table 2. Their values of E_a are very close to each other. The values of E_a and A obtained from a single non-isothermal DSC curve are in good agreement with the calculated values by Kissinger's and Ozawa's methods in Table 3. Therefore, we conclude that the main exothermic decomposition reaction mechanism of ATO is classified as nucleation and growth, and the mechanism function is Avrami–Erofeev equation with n = 3/4 [18]. The reaction mechanism of exothermic main decomposition process of the compound is classified as $f(\alpha) = 3(1-\alpha)[-\ln(1-\alpha)]^{1/4}/4$, $G(\alpha) = [-\ln(1-\alpha)]^{3/4}$.

Substituting $f(\alpha)$ with $3/4(1-\alpha)[-\ln(1-\alpha)]^{1/4}$, E with 119.50 kJ mol^{-1} and A with $10^{9.03}$ s^{-1} in

$$\frac{\mathrm{d}\alpha}{\mathrm{d}T} = \frac{A}{\beta} f(\alpha)\, \mathrm{e}^{-E_a/RT} \tag{10}$$

the kinetic equation of the exothermic decomposition reaction may be described as dα/dT = ($10^{8.91}/\beta$) exp($-1.44 \times 10^4/T$)$(1-\alpha)[-\ln(1-\alpha)]^{1/4}$.

The values T_{po} of the peak temperature (T_p) corresponding to $\beta \to 0$ obtained by Eq. (11) taken from [17] are 276.49 °C:

$$T_p = T_{po} + a\beta_i + b\beta_i^2, \quad i = 1\text{–}4 \tag{11}$$

where a and b are coefficients: a = 4.18067, b = −0.08146.

The corresponding critical temperatures of thermal explosion (T_b) obtained from Eq. (12) taken from [19] is 299.63 °C:

$$T_b = \frac{E_o - \sqrt{E_o^2 - 4E_oRT_{po}}}{2R} \tag{12}$$

where R is the gas constant (8.314 J mol^{-1} K^{-1}), E_o is the value of E obtained by Ozawa's method.

Table 2
Kinetic parameters obtained by the data in Table 1

Eqs.	Mechnism function $f(\alpha)$	E_a (kJ mol^{-1})	log(A) (s^{-1})	r
(5)	$f(\alpha) = 3(1-\alpha)[-\ln(1-\alpha)]^{1/4}/4$	123.96	9.33	0.9978
(6)	$f(\alpha) = 3(1-\alpha)[-\ln(1-\alpha)]^{1/4}/4$	125.21	9.53	0.9978
(7)	$f(\alpha) = 3(1-\alpha)[-\ln(1-\alpha)]^{1/4}/4$	122.44	9.24	0.9974
(8)	$f(\alpha) = 3(1-\alpha)[-\ln(1-\alpha)]^{1/4}/4$	122.44	9.23	0.9974
(9)	$f(\alpha) = 3(1-\alpha)[-\ln(1-\alpha)]^{1/4}/4$	103.45	7.82	0.9973
	Mean	119.50	9.03	

Table 3
Calculated values of the kinetic parameters for the exothermic decomposition reaction of ATO determined from the DSC curves at various heating rates (β)

β (°C min^{-1})	T_P (°C)	E_k (kJ mol^{-1})	log(A_k) (s^{-1})	r_k	Q_k	E_o (kJ mol^{-1})	r_o	Q_o	$\bar{E}_a$ (kJ mol^{-1})
5.85	297.41	114.21	8.05	0.9874	0.0252	117.88	0.9892	0.0479	116.05
12.07	317.34								
18.12	323.34								
24.94	330.74								

β, heating rate; T_p, maximum peak temperature in the DSC curve; A, pre-exponential constant; r, linear correlation coefficient; subscript k, data obtained by Kissinger's method; subscript o, data obtained by Ozawa's method; Q, standard mean square deviation; $\bar{E}_a = (E_k + E_o)/2$.

The entropy of activation ($\Delta S^{\#}$), enthalpy of activation ($\Delta H^{\#}$) and free energy of activation ($\Delta G^{\#}$) corresponding to $T = T_{pdo}$, $E_a = E_k$ and $A = A_k$ obtained by Eqs. (13)–(15) are −95.88 J mol^{-1} K^{-1}, 114.21 kJ mol^{-1} and 166.91 kJ mol^{-1}, respectively:

$$A = \frac{k_B T}{h} e^{\Delta S^{\neq}/R} \tag{13}$$

$$A \exp\left(\frac{-E_a}{RT}\right) = \frac{kT}{h} \exp\left(\frac{\Delta S^{\neq}}{R}\right) \exp\left(-\frac{\Delta H^{\neq}}{RT}\right) \tag{14}$$

$$\Delta G^{\neq} = \Delta H^{\neq} - T\Delta S^{\neq} \tag{15}$$

where k_B is the Boltzmann constant and h the Plank constant.

3.3. The results and discussion in solid reaction cell and gas reaction cell

In the experiment of solid reaction cell *in situ*/RSFT-IR, the sample was heated at a heating rate of 10 °C min^{-1} with KBr pellet samples and the infrared spectrum was recorded by fast scanning. The IR characteristic absorption peak intensity of the condensed phase reactant of ATO with temperature was shown in Fig. 2.

The obvious variation of IR characteristic absorption peaks of ATO at 20 °C (before melting) and 151 °C (after melting) were shown in Fig. 3 and the curves of the corresponding relative intensity of the characteristic groups for ATO at different temperatures were illustrated in Fig. 4.

When the solid was heated to 50 °C, the peak shape of the IR spectra changed slightly and when the temperature reached to 130 °C, the IR characteristic absorption peaks changed rapidly. The characteristic absorption peak of C=O broadened and transferred to 1713 cm^{-1} from 1710 cm^{-1} (Fig. 3). The following obvious peak transformation were occurred with the increase of temperature, the single peak at 1627 cm^{-1} is transformed from the double peaks at 1643 and 1618 cm^{-1}, that at 1224 cm^{-1} is changed from those at

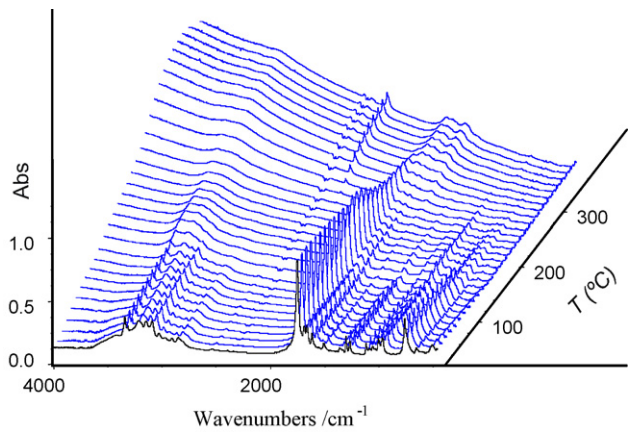

Fig. 2. IR characteristic absorption peak intensity of the condensed phase reactant of ATO vs. temperature (°C).

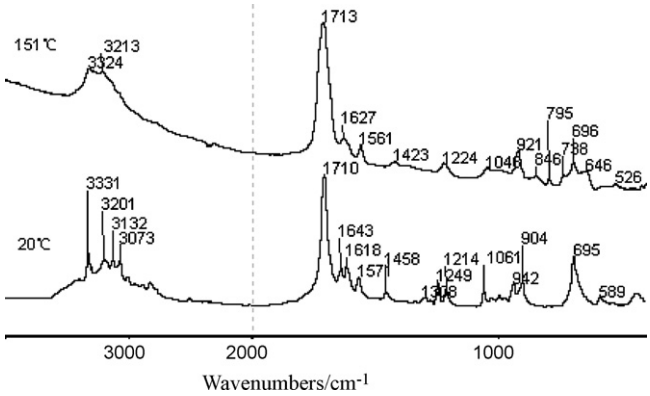

Fig. 3. IR spectra of the condensed phase of ATO at 20 and 151 °C.

1249 and 1214 cm^{-1}, that at 921 cm^{-1} is changed from those at 942 and 904 cm^{-1}, and that at 1046 cm^{-1} is changed from those at 1061 and 1030 cm^{-1}. The curves of the sudden leap of the relative intensity of the characteristic groups are due to the melting of ATO. With the temperature increasing, no IR characteristic absorption peaks of decomposition products appeared because of the sublimation of ATO.

In the RSFT-IR/gas reaction cell, the detector paved with sample (1 mg) was heated to 700 °C at a heating rate of 700 °C s^{-1} using T-Jump technique so that ATO decomposed before sublimation. IR spectra of the gas phase decomposition products of ATO at 1.2, 1.4 and 11.2 s were shown in Fig. 5 and the density distribution of the gas phase decomposition products of ATO was shown in Fig. 6.

It can be seen from the figures that the main products during the thermal decomposition process of ATO are HCN, NH_3, CO and HNCO. With increase of time, the intensity of characteristic absorption peaks of HCN, NH_3, CO and HNCO were decreased while the absorption

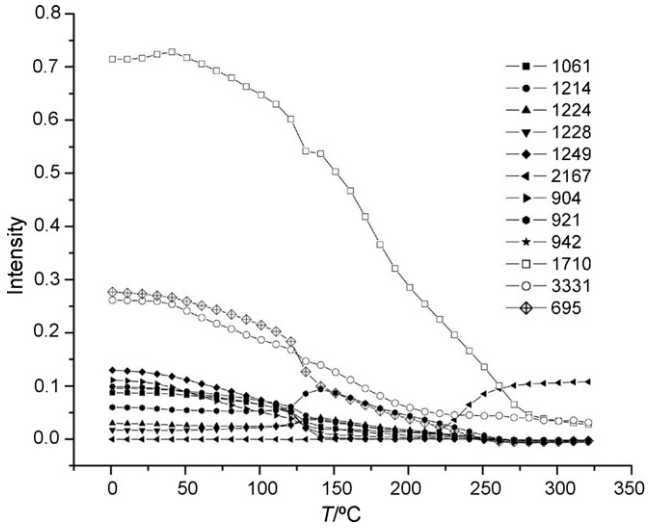

Fig. 4. IR spectra of the condensed phase of ATO at different temperatures (°C).

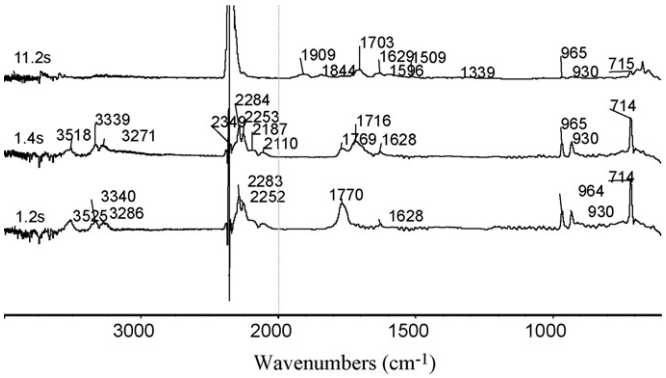

Fig. 5. IR spectra of the gas phase decomposition products of ATO at 1.2, 1.4, and 11.2 s.

peaks of NO at 1909 cm^{-1} and CO_2 at 2349 cm^{-1} are increased with the sublimation products of ATO. Therefore, we can conclude that HCN, NH_3, CO and HNCO are the first decomposition products of ATO, NO and CO_2 are the second decomposition products.

3.4. Heat of formation and detonation properties

It is well known that the performance of energetic materials requires the knowledge of the heat of formation (HOF). Furthermore, HOFs, as elementary thermodynamic properties, are important and necessary for researchers. For stable compounds, there are many tables that contain experimental data of HOFs. However, for energetic materials and unstable compounds, determination of the HOFs is impractical or dangerous. Detonation velocity, detonation pressure (P) are important parameters to evaluate the performances of energetic materials. Quantitative estimation of properties, such as the HOFs, detonation velocity, detonation pressure and sensitivity, would permit the selection of the most promising substances for laboratory synthesis and further consideration.

The HOF for ATO is evaluated to be 83.91 kJ mol^{-1} (larger than the famous 3-nitro-1,2,4-triazol-5-one (NTO), 79.00 kJ mol^{-1} [20]) by G3 theory, based on the atomization energies being used by Curtiss et al. [12].

Therefore, the calculated detonation velocities and detonation pressure are 7064 m/s and 21.1 GPa based on the calculated HOF and the determined crystal density of 1.670 g cm^{-3} [11] by X-ray diffraction analysis, respectively.

4. Conclusion

The thermal decomposition of ATO is composed of a melting process and an exothermic decomposition process in the sealed stainless steel cells. The main exothermic decomposition reaction mechanism of ATO is classified as nucleation and growth, and the mechanism function is Avrami–Erofeev equation with $n = 3/4$. The kinetic parameters of the reaction are $E_a = 119.50$ kJ mol^{-1} and $A = 10^{9.03}\ s^{-1}$, the kinetic equation can be described as $d\alpha/dT = (10^{8.91}/\beta)\exp(-1.44 \times 10^4/T)(1-\alpha)[-\ln(1-\alpha)]^{1/4}$. HCN, NH_3, CO and HNCO are the first decomposition products of ATO. The calculated heat formation of ATO is 83.91 kJ mol^{-1} and the calculated detonation velocities (D) and detonation pressure (P) are 7064 m/s and 21.1 GPa, respectively.

Acknowledgements

This work is supported by the National Natural Science Foundation of China (20603026), the Backbone Teacher of Chinese University Sustentation Fund of the Ministry of Education PR China, the Education Committee Foundation of Shaanxi Province (6JK172) and the Provincial Natural Foundation of Shaanxi (2005B15).

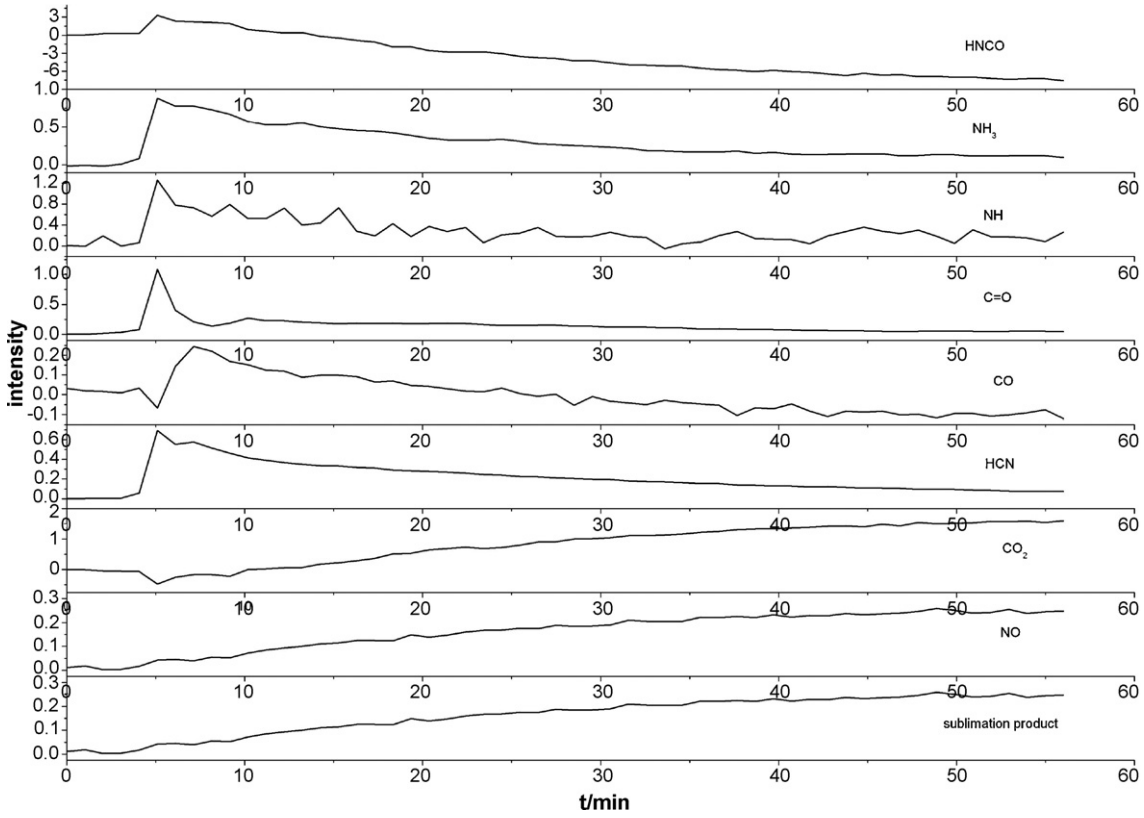

Fig. 6. The density distribution of the gas phase decomposition products of ATO.

Appendix A

Forty-one kinetic functions used for the present analysis

No.	Name of function	Mechanism	$G(\alpha)$	$f(\alpha)$
1	Parabola law	One-dimensional diffusion, 1D	α^2	$\alpha^{-1/2}$
2	Valensi equation	Two-dimensional diffusion, 2D	$\alpha + (1-\alpha)\ln(1-\alpha)$	$[-\ln(1-\alpha)]^{-1}$
3	Jander equation	Two-dimensional diffusion, 2D, $n = 1/2$	$[1-(1-\alpha)^{1/2}]^{1/2}$	$4(1-\alpha)^{1/2}[1-(1-\alpha)^{1/2}]^{1/2}$
4	Jander equation	Two-dimensional diffusion, 2D, $n = 2$	$[1-(1-\alpha)^{1/2}]^2$	$(1-\alpha)^{1/2}[1-(1-\alpha)^{1/2}]^{-1}$
5	Jander equation	Three-dimensional diffusion, 3D, $n = 1/2$	$[1-(1-\alpha)^{1/3}]^{1/2}$	$6(1-\alpha)^{2/3}[1-(1-\alpha)^{1/3}]^{1/2}$
6	Jander equation	Three-dimensional diffusion, spheres symmetry, 3D, $n = 2$	$[1-(1-\alpha)^{1/3}]^2$	$3(1-\alpha)^{2/3}[1-(1-\alpha)^{1/3}]^{-1}{}_{/2}$
7	G.-B. equation[a]	Three-dimensional diffusion, 3D	$1-2\alpha/3-(1-\alpha)^{2/3}$	$3(1-\alpha)^{-1/3}-1]^{-1}/2$
8	Anti-Jander equation	Three-dimensional diffusion, 3D	$[(1+\alpha)^{1/3}-1]^2$	$3(1+1)^{2/3}[(1+\alpha)^{1/3}-1]^{-1/2}$
9	Z.-L.-T. equation[b]	Three-dimensional diffusion, 3D	$[(1-\alpha)^{-1/3}-1]^2$	$3(1-\alpha)^{4/3}[(1-\alpha)-^{1/3}-1]^{-1/2}$
10	Avrami–Erofeev equation	Assumes random nucleation and its subsequent growth, $n = 1/4$, $m = 4$	$[-\ln(1-\alpha)]^{1/4}$	$4(1-\alpha)[-\ln(1-\alpha)]^{3/4}$
11	Avrami–Erofeev equation	(Same as above) $n = 1/3$, $m = 3$	$[-\ln(1-\alpha)]^{1/3}$	$3(1-\alpha)[-\ln(1-\alpha)]^{2/3}$
12	Avrami–Erofeev equation	(Same as above) $n = 2/5$	$[-\ln(1-\alpha)]^{2/5}$	$5(1-\alpha)[-\ln(1-\alpha)]^{3/5}/2$
13	Avrami–Erofeev equation	(Same as above) $n = 1/2$, $m = 2$	$[-\ln(1-\alpha)]^{1/2}$	$2(1-\alpha)[-\ln(1-\alpha)]^{1/2}$
14	Avrami–Erofeev equation	(Same as above) $n = 2/3$	$[-\ln(1-\alpha)]^{2/3}$	$3(1-\alpha)[-\ln(1-\alpha)]^{1/3}/2$
15	Avrami–Erofeev equation	(Same as above) $n = 3/4$	$[-\ln(1-\alpha)]^{3/4}$	$3(1-\alpha)[-\ln(1-\alpha)]^{1/4}/4$
16	Avrami–Erofeev equation	(Same as above) $n = 1$, $m = 1$	$[-\ln(1-\alpha)]^{3/2}$	$1-\alpha$
17	Avrami–Erofeev equation	(Same as above) $n = 3/2$	$-\ln(1-\alpha)$	$2(1-\alpha)[-\ln(1-\alpha)]^{-1/2}/3$
18	Avrami–Erofeev equation	(Same as above) $n = 2$	$[-\ln(1-\alpha)]^2$	$(1-\alpha)[-\ln(1-\alpha)]^{-1}/2$
19	Avrami–Erofeev equation	(Same as above) $n = 3$	$[-\ln(1-\alpha)]^3$	$(1-\alpha)[-\ln(1-\alpha)]^{-2}/3$
20	Avrami–Erofeev equation	(Same as above) $n = 4$	$[-\ln(1-\alpha)]^4$	$(1-\alpha)[-\ln(1-\alpha)]-^3/4$
21	P.-T. equation[c]	Autocatalysis, branch random nucleation	$-\ln[\alpha/(1-\alpha)]$	$\alpha(1-\alpha)$
22	Mampel power law	$n = 1/4$	$\alpha^{1/4}$	$4\alpha^{3/4}$
23	Mampel power law	$n = 1/3$	$\alpha^{1/3}$	$3\alpha^{2/3}$
24	Mampel power law	$n = 1/2$	$\alpha^{1/2}$	$2\alpha^{1/2}$
25	Mampel power law	Phase boundary reaction, R_1, $n = 1$	α	1
26	Mampel power law	$n = 3/2$	$\alpha^{3/2}$	$2\alpha^{-1/2}/3$
27	Mampel power law	$n = 2$	α^2	$\alpha^{-1}/2$
28	Reaction order	$n = 1/4$	$1-(1-\alpha)^{1/4}$	$4(1-\alpha)^{3/4}$
29	Contracting	Phase boundary reaction, R_3	$1-(1-\alpha)^{1/3}$	$3(1-\alpha)^{2/3}$
30	Sphere (volume)	$n = 1/3$, $n = 3$ (three-dimension)	$3[1-(1-\alpha)^{1/3}]$	$(1-\alpha)^{2/3}$
31	Contracting cylinder	Phase boundary reaction, R_2	$1-(1-\alpha)^{1/2}$	$2(1-\alpha)^{1/2}$
32	(Area)	$n = 1/2$, $n = 2$ (two-dimension)	$2[1-(1-\alpha)^{1/2}]$	$(1-\alpha)^{1/2}$
33	Reaction order	$n = 2$	$1-(1-\alpha)^2$	$(1-\alpha)^{-1}/2$
34	Reaction order	$n = 3$	$1-(1-\alpha)^3$	$(1-\alpha)^{-2}/3$
35	Reaction order	$n = 4$	$1-(1-\alpha)^4$	$(1-\alpha)^{-3}/4$
36	Second order	Chemical reaction, F_2	$(1-\alpha)^{-1}$	$(1-\alpha)^2$
37	Reaction order	Chemical reaction	$(1-\alpha)^{-1}-1$	$(1-\alpha)^2$
38	2/3 order	Chemical reaction	$(1-\alpha)^{-1/2}$	$2(1-\alpha)^{3/2}$
39	Exponent law	E_1, $n = 1$	$\ln\alpha$	α
40	Exponent law	$n = 2$	$\ln\alpha^2$	$\alpha/2$
41	Third order	Chemical reaction, F_3	$(1-\alpha)^{-2}$	$(1-\alpha)^3/2$

[a] Ginstling–Brounshtein equation.
[b] Zhuralev–Lesokin–Tempelman equation.
[c] Prout–Tompkins equation.

References

[1] C.F. Kroeger, L. Hummel, M. Mutscher, H. Beyer, Berichte der Deutschen Chemische Gcsellschaft 98 (1965) 3025.
[2] K.M. Dusseldorf, K.K. Odenthal, P.H. Dormagen, USP 4 952 701 (1990).
[3] K.K. Odenthal, K.M. Dusseldorf, L.R. Wuppertal, USP 5 034 538 (1991).
[4] K.K. Odenthal, K.M. Dusseldorf, L.R. Wuppertal, USP 5 153 326 (1992).
[5] A. Bernardini, P. Vialleofont, Org. Mass Spectrom. 14 (1970) 369.
[6] J.G. Zhang, T.L. Zhang, Chin. J. Phys. Chem. 16 (2000) 1110 (in Chinese).
[7] J.G. Zhang, T.L. Zhang, Acta Chim. Sin. 58 (2000) 1563 (in Chinese).
[8] T.L. Zhang, J.G. Zhang, Z.G. Zhang, K.B. Yu, Acta Chim. Sin. 58 (2000) 533 (in Chinese).
[9] J.G. Zhang, Studies on Triazol Heterocyclic Compounds and Their Complexes [D], Beijing Institute of Technology, Beijing, 2000 (in Chinese).
[10] J.G. Zhang, T.L. Zhang, Huozhayaoxuebao 2 (2001) 19 (in Chinese).
[11] H.X. Ma, H.M. Xiao, J.R. Song, X.H. Ju, W. Zhu, K.B. Yu, Chem. Phys. 344 (2008) 79.
[12] L.A. Curtiss, M.P. McGrath, J.P. Blaudeau, N.E. Davis, R.C. Binning Jr., L. Radom, J. Chem. Phys. 103 (1995) 6104.
[13] M.J. Frisch, G.W. Trucks, H.B. Schlegel, G.E. Scuseria, M.A. Robb, J.R. Cheeseman, V.G. Zakrzewski, J.A. Montgomery, R.E. Stratmann, J.C. Burant, S. Dapprich, J.M. Millam, A.D. Daniels, K.N. Kudin, M.C. Strain, O. Farkas, J. Tomasi, V. Barone, M. Cossi, R. Cammi, B. Mennucci, C. Pomelli, C. Adamo, S. Clifford, J. Ochterski, G.A. Petersson, P.Y. Ayala, Q. Cui, K. Morokuma, D.K. Malick, A.D. Rabuck, K. Raghavachari, J.B. Foresman, J. Cioslowski, J.V. Ortiz, B.B. Stefanov, G. Liu, A. Liashenko, P. Piskorz, I. Komaromi, R. Gomperts, R.L. Martin, D.J. Fox, T. Keith, M.A. Al-Laham, C.Y. Peng, A. Nanayakkara, C. Gonzalez, M. Challacombe, P.M.W. Gill, B.G. Johnson, W. Chen, M.W. Wong, J.L. Andres, M. Head-Gordon, E.S. Replogle, J.A. Pople, Gaussian 98 (Revision A.7), Gaussian, Inc., Pittsburgh, PA, 1998.
[14] M.J. Kamlet, S.J. Jacobs, J. Chem. Phys. 48 (1968) 23.
[15] H.E. Kissinger, Anal. Chem. 29 (1957) 1702.
[16] T. Ozawa, Bull. Chem. Soc. Jpn. 38 (1965) 1881.
[17] R.Z. Hu, Z.Q. Yang, Y.J. Liang, Thermochim. Acta 123 (1988) 135.
[18] R.Z. Hu, Q.Z. Shi, Thermal Analysis Kinetics, Science Press, Beijing, 2001, p. 127 (in Chinese).
[19] T.L. Zhang, R.Z. Hu, Y. Xie, F.P. Li, Thermochim. Acta 244 (1994) 171.
[20] K.Y. lee, M.D. Coburn, US Patent 4733610 (1988).